Head-on collisions of unequal mass black holes: close-limit predictions

Zeferino Andrade and Richard H. Price
Department of Physics, University of Utah, Salt Lake City, UT 84112

The close-limit method has given approximations in excellent agreement with those of numerical relativity for collisions of equal mass black holes. We consider here colliding holes with unequal mass, for which numerical relativity results are not available. We try to ask two questions: (i) Can we get approximate answers to astrophysical questions (ideal mass ratio for energy production, maximum recoil velocity, etc.), and (ii) can we better understand the limitations of approximation methods. There is some success in answering the first type of question, but more with the second, especially in connection with the issue of measures of the intrinsic mass of the colliding holes, and of the range of validity of the method.

arXiv:gr-qc/9611022v1 9 Nov 1996

I. INTRODUCTION AND OVERVIEW

Recently much attention has been given to the problem of the collision of two black holes. There are two main reasons for such interest. First, black hole collisions provide one of the most powerful and interesting sources for possible detection by gravitational wave observatories [1]. Second, black hole collisions are being intensively studied numerically by using supercomputers to evolve Einstein's equations from initial data representing two holes [2].

The enormous difficulty of solving the equations numerically provides motivation for approximation methods that, with little effort, can give guidance to what results can be expected, what cases are interesting for full numerical study, etc. One method that has proved surprisingly successful in a range of tests is the close-limit approximation (CLAP). This method applies to initial value data representing holes which are initially close to each other. If the holes are close enough then the horizon will initially surround both holes, and the spacetime outside the horizon can be considered to be a single perturbed hole. Strong nonsphericity inside the initial horizon cannot affect the evolution of the fields outside, and hence does not influence the generation of outgoing radiation. The nonspherical perturbations outside the horizon can be analyzed with the well developed techniques of linear perturbation theory.

The method, applied to numerically or analytically generated initial data was discussed by Abrahams and Price [3], and has been applied to: (i) simple analytic initial data for the head-on collision of momentarily stationary black holes [4–6], (ii) numerically generated initial value data for holes which are initially moving towards each other [7], (iii) analytic initial value solutions for holes which are initially moving slowly towards each other [8], (iv) analytic initial data for holes which have opposite inital angular momentum and are initially momentarily stationary [9]. Where comparisons with full numerical results are available (all of the applications above, except the last) the results of the CLAP method are found to be remarkably successful, even when initial conditions would seem to violate the assumptions underlying the approximations. This success holds the promise of giving easy approximate answers about black hole collisions.

All applications listed above have been to collisions of holes with equal masses. (Those are essentially the only cases for which comparisons have been available with fully numerical computations.) Here we consider collisions of unequal mass holes, though comparisons with numerical results cannot yet be made. There are two reasons we do this. First, there are some interesting questions to which it is better to have a very rough answer, even an uncertain answer (if the nature of the uncertainty is kept in mind), than no answer at all. It is interesting to see whether there are any surprises in predicted radiation efficiency, in dependence on details of initial data, etc. One interesting question applies *only* when the masses are unequal: can gravitational radiation from the collision contain a significant amount of linear momentum, so that the hole that forms will recoil with an astrophysically significant proper velocity?

The second motivation is to look at the range of validity of CLAP calculations. The ultimate index of validity (short of full numerical relativity comparisons) is second-order perturbation calculations, and work on this technique is well underway [10,11]. These necessary calculations, however, are quite difficult (though far easier than full numerical computations) and it is useful to look at whether simple guidelines exist. Our approach here is simultaneously to use the CLAP method to look for astrophysical answers, and to use the examples to gain deeper understanding of the method.

The nature of the questions being asked justifies avoiding unnecessary complications and using the simplest initial data sets applicable. We therefore limit our attention here to nonspinning holes which start from rest and undergo a head-on collision. More specifically, we limit our investigation to two momentarily stationary initial solutions. Both

initial geometries are conformally flat, and therefore are completely determined by a conformal factor Φ^4, where Φ solves the flat spacetime Laplace equation [12]. The simplest solution is that of Brill and Lindquist [13] (hereafter "BL") in which Φ has the form of the gravitational potential for two Newtonian point masses. Another solution, that of Misner and Lindquist [14–16] (hereafter "ML") is more complicated but has the very useful feature of an easily located minimal area of the Einstein-Rosen bridges in the initial geometry. It is also the initial geometry that has been used in almost all numerical relativity studies of collisions of black holes. For these two sets of initial data we look at radiated energy as a function of how close the initial holes are. To characterize the separation of the holes, we use in all cases the proper distance L, along the symmetry axis, between the apparent horizons of each of the holes.

An important issue that arises is how to characterize the "bare mass" of each of the throats, i.e., how to assign an intrinsic mass to each of the holes participating in the collision, a mass unaffected (in some sense) by the presence of other nearby sources of gravitation. There is a fairly natural choice of bare mass for the BL initial data, but not for the ML initial data. We consider three candidates as bare mass measures in the ML case. One of the more interesting conclusions of this work is the importance of the choice of bare mass, and the unphysical consequences of the wrong choice.

In Sec. II we start by describing the BL and ML solutions and the choices that can be made for bare mass. We then describe the CLAP method. CLAP estimates of radiated energy are presented in Sec. III where it is seen that the choice of bare mass of one ML hole governs even the qualitative nature of some answers. In Sec. IV results are given for the recoil velocity of the final hole formed, due to the emission of radiation. In the results of Secs. III and IV, the usefulness of the results depend heavily on the range of validity of the CLAP. In Sec. V we look at a simple criterion for when linearized theory should be applicable. We find that the validity of this criterion, which seems useful in the case of equal mass holes, does not seem to extend to collisions in which the ratio of hole masses is very small. Conclusions are presented in Sec. VI. Details of several calculations are presented in three appendices.

II. APPROXIMATION METHOD AND INITIAL GEOMETRIES

Initial value solutions

For simplicity we limit attention to time symmetric initial data. There is then an initial hypersurface on which the extrinsic curvature is zero so that initial value data for Einstein's equations consists only of the three geometry of this hypersurface. Also for simplicity, we limit our consideration to three geometries that are conformally flat. This simplification is neither selected for or against by any strong physical argument, but it leads to a very convenient mathematical description, and is therefore used, e.g., in most numerical relativity work.

We write the conformally flat axisymmetric three metric in the form

$$ds^2 = \Phi^4(R,\theta)(dR^2 + R^2 d\Omega^2) \ , \tag{1}$$

where $d\Omega^2 = d\theta^2 + d\varphi^2 \sin^2\theta$, and R, θ, φ are spherical coordinates in the flat conformal space. The Einstein initial value equations then turn out to require only that Φ obey Laplace's equation

$$\nabla^2 \Phi = 0 \ , \tag{2}$$

where ∇^2 is the Laplacian with respect to the flat metric $dR^2 + R^2 d\Omega^2$.

It is necessary to find solutions corresponding to two initially static black holes. To investigate the possible sensitivity of radiation to the details of the initial value solution we consider two different solutions of (2). Brill and Lindquist investigated the solution to (2) that is most immediately apparent [13], the solution with the form of the Newtonian gravitational potential of two mass points:

$$\Phi = 1 + \frac{\alpha_1}{|\vec{R} - \vec{R}_1|} + \frac{\alpha_2}{|\vec{R} - \vec{R}_2|} \ . \tag{3}$$

Here all the vectors and their norms are defined in the flat three dimensional space, with $\vec{R}$ being the position of an arbitrary point in such space and $\vec{R}_i$ is the position of a point in the flat space representing hole i. Though (3) suggests two pointlike solutions, there are in fact no physical singularities corresponding to these points. Rather the three geometry near each "point" can be extended, through a throat, out to an asymptotically flat space (an Einstein-Rosen bridge). The complete BL three geometry, then, includes three asymptotically flat regions. One is a region with two throats connected, the region of "our universe." The other two regions contain one throat each corresponding to mass 1, and to mass 2. (These distinctions are meaningful only when the two throats are well separated in "our" universe; see [13]).

The BL topology has a useful practical feature. Since hole 1 (for example) has its own asymptotically flat region we can infer a "bare mass" m_1 for hole 1 from the metric at large distances from the throat. In this way we can compute bare masses m_i for each of the individual holes. (In the limit that the holes are very far apart, the bare masses are related to the parameters α_i in (3) by $\alpha_i \approx m_i/2$, where we use $c = G = 1$ units.) We can also compute the total mass M in "our" universe, the ADM mass of the two-hole spacetime.

Another solution to (2), corresponding to two throats, of the form

$$\Phi = 1 + \sum_{n=1}^{\infty} \left(\frac{a_n}{|\vec{R} - \vec{d}_n|} + \frac{b_n}{|\vec{R} - \vec{e}_n|} \right) , \tag{4}$$

can be constructed by placing the "masses" a_n and b_n at the locations $\vec{d}_n$ and $\vec{e}_n$ in the flat conformal three geometry in a manner similar to the placement of electrical charges in the problem of finding the electric potential distribution in the region outside two charged conducting spheres. With an infinite set of image "masses" it is possible to construct a three geometry with two throats which open into two identical asymptotically flat regions. The isometry between the two regions takes the form of a reflection through spheres at the minimal neck of each of the throats. The details of the symmetrization procedure are given in Appendix B (see also Lindquist [16]).

For our purposes, the disadvantage of ML solutions is that there is no immediate meaning that can be given to "bare mass." We consider three candidates for bare mass in ML solutions. One candidate is the bare mass suggested by Lindquist in his study of symmetrized initial value solutions [16]. The "Lindquist mass" sums the bare masses of all the images associated with one of the throats (a divergent sum) then subtracts a Newtonian expression for the binding energy due to the interaction of those images with each other (another divergent sum). This definition of bare mass seems not to have been used in recent work on the problem. Much more commonly cited is a rather straightforward measure of the bare mass that we shall call the "area-mass." One takes the area A_i of the minimal throat on the initial hypersurface and computes a bare mass from it as if it were an isolated Schwarzschild horizon: $m_i = \sqrt{A_i/16\pi}$. A third candidate for the bare mass is the "Penrose mass" [17–19]. This is a quasi-local definition of mass interior to a 2-sphere that starts with a method, valid in linearized theory, of extracting mass information from the Weyl tensor. This method is then formally converted to curved spacetime. The method, cannot be applied to all spacetimes, but it is always applicable to axisymmetric cases. Some details of the computation of the Penrose mass are given in Appendix C.

FIG. 1. For two holes with fixed Penrose mass m_{iP}, in the ratio $m_{2P}/m_{1P} = 3/7$, the dependence of the Lindquist mass m_{iL} on separation is shown.

Figure 1 illustrates the issue of choice of bare mass in the ML case with an example in which the ratio of Penrose bare masses of the two holes is 7:3. For each hole, the ratio of Lindquist mass to Penrose mass is shown as a function of separation. For both the heavy and the light holes, the Lindquist mass decreases relative to the Penrose mass, but the decrease is more dramatic for the heavy hole. If the statement "put the same two holes at different separation" means putting holes of fixed Penrose mass at different separations, then these "same" two holes at small separation have very different Lindquist masses, and a very different ratio of Lindquist masses. A similar comparison between Lindquist mass and area-mass tells a very different story. If the m_1/m_2 ratio of area-mass is 7:3 then, to considerable accuracy, the ratio of Lindquist masses is also 7:3. There is not a strict equivalence of the two ratios. At very small separation there is a small deviation in the ratios. More important, the value of the Lindquist mass and that of the area-mass for a given hole are not the same when separations are small, but even here the effects are small. This is shown in Fig. 2 for two equal mass hole. At small distances (L/M less than around 0.5) the Lindquist mass is discernibly larger than the area-mass. By comparison, the difference in Penrose mass and area-mass is 20 times larger. In our energy and recoil estimates in the next two sections, no difference can be seen in the results depending on which mass ratio is held constant, the Lindquist mass or the area-mass. We shall, therefore, present only the latter.

FIG. 2. Difference between Lindquist and area mass as a function of separation when the holes are equal. Here M is the total ADM mass of the spacetime.

FIG. 3. For the bare mass m_2 of a hole, the ratio of the Penrose measure of bare mass (m_{2P}) to the Lindquist measure (m_{2L}) is shown as a function of the ratio of (Lindquist) bare masses for two different separations L/M (where M is the total ADM mass of the spacetime). The result shows that in the extreme ratio limit different measures of bare mass agree.

In the limit of extreme mass ratio (as well as in the limit of large separation) the ambiguities of bare mass disappear. When the limit m_2/m_1 of the bare masses becomes very small, the "particle" limit for m_2, physical intuition suggests

that any reasonable definition of bare mass must agree with the proper mass of a point particle perturbing the spacetime, and therefore all reasonable definitions of bare mass will yield the same result. This is illustrated in Fig. 3, which shows the ratio of the Penrose and Lindquist measures of m_2, the bare mass of the less massive hole, as the ratio of bare masses m_2/m_1 goes to zero. It is clear that in this limit also all reasonable measures of m_1, the bare mass of the more massive hole, will agree with each other and with the ADM mass of the spacetime. As a check we have computed the ratio of Penrose to Lindquist values of m_1 as m_2/m_1 decreases and have verified that the ratio goes to unity (although not as quickly as in Fig. 3).

The close approximation

To apply the CLAP to the momentarily stationary axisymmetric space we must rewrite (1) in the form of a $t \approx$ constant slice of a Schwarzschild spacetime. This requires mapping the geometry of (1) onto a set of Schwarzschild-like coordinates r, θ, φ. We do this by transforming the radial coordinate as if R were the isotropic radial coordinate for the Schwarzschild geometry:

$$R = (\sqrt{r} + \sqrt{r - 2M})^2/4 \ , \tag{5}$$

where M is the total mass of the spacetime. This transformation puts the spatial metric in the form

$$ds^2 = \mathcal{F}^4 \left(\frac{dr^2}{1 - 2M/r} + r^2 d\Omega^2 \right) \ , \tag{6}$$

where

$$\mathcal{F} \equiv \frac{\Phi(R, \theta)}{1 + M/2R} \ . \tag{7}$$

The function Φ must satisfy (2) and will have singularities at the coordinate locations R_i of "mass points"(BL) or "images"(ML). Since Φ must approach the Schwarzschild spatial metric $\Phi \to 1 + 2M/R$ as $R \to \infty$, we can expand Φ, for $R > \max(R_i)$, in Legendre polynomials P_ℓ as

$$\Phi = 1 + \frac{2M}{R} + \sum_{\ell=1}^{\infty} \gamma_\ell \left(\frac{M}{R} \right)^{\ell+1} P_\ell(\cos\theta) \ . \tag{8}$$

We can eliminate the $\ell = 1$ term from (8) by appropriate choice of coordinate origin. The expression for $\mathcal{F}$, therefore, can be put into the form

$$\mathcal{F} = 1 + \frac{1}{1 + M/2R} \sum_{\ell=2}^{\infty} \gamma_\ell \left(\frac{M}{R} \right)^{\ell+1} P_\ell(\cos\theta) \ . \tag{9}$$

For an initial value solution representing two black holes, the coefficients γ_ℓ will contain a parameter describing the separation of the holes. As the separation goes to zero, the geometry approaches that of a $t =$ constant slice of the Schwarzschild geometry, and the γ_ℓ must therefore all approach zero. The close approximation consists of treating the separation of the holes as a perturbation parameter and in (9) keeping only the terms lowest order in the separation. When we take the fourth power of $\mathcal{F}$ the mixing of the P_ℓ gives us, in principle, very complicated mixtures of contributions of different ℓ for each final multipole of $\mathcal{F}^4$. The result in practice is much simpler. For both the BL and ML solutions (in fact for any conformally flat metric (1) for which (5) is used) the γ_ℓ coefficients increase in the order of the perturbation as ℓ increases and, as a result, for each ℓ-pole of $\mathcal{F}^4$ the contribution of lowest perturbative order is due only to the γ_ℓ term, and the conformal factor can be written

$$\mathcal{F}^4 = 1 + \frac{4}{1 + M/2R} \sum_{\ell=2}^{\infty} \gamma_\ell \left(\frac{M}{R} \right)^{\ell+1} P_\ell(\cos\theta) \ . \tag{10}$$

Equations (5), (6), and (10) describe an initial perturbation of the Schwarzschild geometry. Following the prescription of Moncrief [20], we can use this perturbed initial solution to give us, for each ℓ, the initial value of a "Zerilli function" [21] ψ_ℓ. (We use the normalization of Abrahams and Price [3], our ψ_ℓ being their Q^+_ℓ.)

This Zerilli function satisfies a simple wave equation and from its initial value it is simple to find the time evolved function $\psi(t,r)$. Once this is known we can compute the gravitational energy radiated by the system of two black holes from

$$\frac{E}{2M} = \frac{1}{32\pi}\sum_{\ell=2}^{\infty}\int dt|\frac{d\psi_\ell}{dt}|^2\frac{1}{2M} \tag{11}$$

It can easily be shown that the Zerilli functions corresponding to two different solutions A and B of (2) differ only in amplitude, i.e. they are related through

$$\psi_\ell^B(r,t) = \frac{\gamma_\ell^B}{\gamma_\ell^A}\psi_\ell^A(r,t) \tag{12}$$

This means that if we know $\psi_\ell(r,t)$ for a given solution of (2), say the Misner equal mass solution, we can compute the energy (Sec. III) and the recoil velocity (Sec. IV) for any other conformally flat solution, directly.

III. RADIATED ENERGY

We give here the radiated energy corresponding to a range of head on collisions. To choose a particular black hole collision, we must first say whether the initial data is BL or ML. Second, we must specify a ratio of hole bare masses, and third we must specify L the separation of the holes, i.e., the proper distance between the apparent horizons. Our results are plotted with the radiated energy and the separation L normalized by the sum of the bare masses, so that the results can be interpreted as showing the change of radiation with separation when the "same" two holes are moved closer together.

For ML holes we consider several different definitions of bare mass, and in Fig. 4 show the results for the Penrose

FIG. 4. For two ML holes, with bare mass ratio $F \equiv m_2/m_1$, the radiated energy is shown as a function of the proper separation L between the apparent horizons. Results are shown for both the Penrose bare mass definition and the Lindquist definition. For extreme mass ratios the choice of bare mass is irrelevant, but for $F = 0.75$ a qualitatively different dependence on separation shows up.

definition and the Lindquist (equivalently, the area) meaning of bare mass. To avoid cluttering the plot the results for $F = 1$ have been omitted. These $F = 1$ results show little difference depending on the choice of bare mass definition. The $F = 1$ curves are only slightly different for Penrose and Lindquist mass, and both are qualitatively similar to the results for $F = 0.75$, with Penrose mass.

The results in Fig. 4 for $F = 0.01$ show the expected independence of bare mass definition. But they fail to show another important feature that has appeared in a study of the particle limit [22]. For particles that fall, starting from rest at distance L from a Schwarzschild hole, here is an anomalous decrease of radiation with decreasing L. This is found only in the range $L = 5M$ to $7M$, where M is the total ADM mass of the spacetime. This unexpected reversal of the general trend is a manifestation of the role played by the "curvature potential" (due to strong field effects near the hole) which peaks at around $L = 3M$.

For our $F = 0.01$ results the ADM mass should be negligibly different from $m_1 + m_2$. So the plot of radiated energy should show this effect in Fig. 4. The fact that it does not can be ascribed to failure of the close limit. We know in fact that this is the case from the study of the particle limit [22]. For extreme mass ratios the close limit will work only for L less than about $2M$, and when it applies the radiation decreases with decreasing L.

For equal mass holes there is no anomalous region. Radiated energy is a monotonic function of initial separation. This can be interpreted to mean that when the smaller hole is not at the particle limit it is "too large" to be situated in the narrow range of radii for which the anomalous energy-separation behavior occurs. As we decrease the bare mass ratio F from unity, there must be some value at which the anomalous region appears. The results in Fig. 4 are interesting in connection with this. For $F = 1$ it is well established that close limit results are reasonably accurate for values of L/M around 4. It would suggest that the anomalous behavior seen at rather small L for the $F = 0.75$ is not an artifact of the close limit. The dramatic low-L bump in that curve, of course, has no counterpart in the corresponding Penrose curve, which suggests that what we are seeing is an effect due to an anomalous choice of bare mass.

FIG. 5. For two BL holes, with bare mass ratio $F \equiv m_2/m_1$, the radiated energy is shown as a function of the proper separation L between the apparent horizons.

For BL collisions, as explained in the previous section, there is a "favored" definition of bare mass. It is straightforward in principle and easy in practice to compute a reasonable mass of each hole by going to large distances in the asymptotically flat region in which that hole is the only throat. For this definition of bare mass, Fig. 5 shows the radiated energy as a function of L, with no anomalous behavior. This supports the argument that the low-L bump, for the Lindquist $F = 0.75$ curve in Fig. 4 is due to an unphysical choice of bare mass.

IV. RECOIL VELOCITY

For unequal mass holes colliding along the z axis there will be momentum contained in the outgoing radiation due to the interaction of multipoles of different ℓ. Moncrief [23] has considered a similar effect in the radiation emitted by a collapsing star.

The general expression for the rate at which z momentum, is radiated is given by

$$\frac{dP^z}{dt} = \frac{1}{16\pi}\sum_{l=2}^{\infty}\sqrt{\frac{(l-1)(l+3)}{(2l+1)(2l+3)}}\frac{d\psi_l}{dt}\frac{d\psi_{l+1}}{dt} \ . \tag{13}$$

The mixture of $\ell = 2$ and 3 is dominant in the sum (13) when the holes start close but the next mixture becomes more and more important as they start farther and farther apart. As a result of radiation emission, the final hole formed will aquire a velocity (relative to the asymptotic frame in which the colliding holes were initially at rest). This recoil velocity is

$$v^z = -\frac{1}{M}\int dt \frac{dP^z}{dt}. \tag{14}$$

In terms of (13) the recoil velocity is

$$v^z = -\frac{1}{16\pi}\sum_{l=2}^{\infty}\sqrt{\frac{(l-1)(l+3)}{(2l+1)(2l+3)}} \times \int \frac{d\psi_l}{dt}\frac{d\psi_{l+1}}{dt}\frac{1}{M}\,dt \ . \tag{15}$$

Now the Zerilli functions $\psi_\ell(t)$ and $\psi_{\ell+1}(t)$ must be evolved numerically and the overlap integral in (15) must be numerically computed. The functions $\psi_\ell(t)$ and $\psi_{\ell+1}(t)$ have a fixed form and the details of the collision influence only the amplitude. The overlap integral in (15) therefore needs to be integrated only once. [See (12).]

This recoil velocity is always negative. Since our convention is always to put the more massive of the colliding holes on the positive z axis and the less massive on the negative side, this means that the final hole moves in the direction from which the smaller mass approached. Results are shown in Fig. 6 for the recoil velocity, in the case of BL initial data, as a function of separation.

FIG. 6. Recoil velocity for BL holes. The recoil velocity of the final hole is shown as a function of initial separation for several ratios of bare mass.

At the low values of L at which the CLAP should be reliable, the highest values of recoil velocity occur for $F \sim 0.3$. The recoil velocity results for ML initial conditions, shown in Fig. 7 are roughly similar. Mass ratios $F \sim 0.1 - 0.3$ produce the highest recoil velocities.

FIG. 7. For two ML holes the recoil velocity of the final hole formed is shown as a function of initial separation, for several different values of F, the ratio of Penrose bare masses.

The figures both for ML and BL initial conditions include recoil velocities of many hundreds of km/sec, proper velocities that would be astrophysically interesting. The large values of v^z correspond, of course, to large initial separations. Whether Figs. 6 and or 7 actually contain results of astrophysical interest depends on whether the CLAP fails at the separations which predict large recoils. This question then, gives us a very specific motivation for turning, in the next section to a consideration of the range of applicability of CLAP.

V. RANGE OF VALIDITY OF CLAP

There is nothing inherent in the linear perturbation theory underlying the CLAP to indicate how small the expansion parameter ϵ must be to have answers accurate to, say, 10%. In other words, we do not immediately know "how close is close enough." The only *a priori* justifiable way of finding the range of validity (aside of course from full numerical solutions) is carry out second-order perturbation theory, and to see at what ϵ the first and second-order answers differ. The formalism for higher order computations has been developed [10], and successfully applied to the equal mass case [11]. Higher order perturbation theory, though much easier than full numerical solutions, is lengthy and tedious. For this reason it is useful to look for easy rough indices of validity of CLAP.

To understand the importance of an index of validity one can look at the application of CLAP to the collision of equal mass ML holes [4,5]. Here a comparison can be made with the results of full nonlinear numerical analysis. Both methods predict an increase of radiation with increasing initial separation. The computed energies agree reasonably well (within a factor of ~ 2) for initial separations out to around $L/M \sim 4$. The energy for infall from extremely large distances is larger only by a factor $\sim 2-3$. It may be that these features are generally true: the magnitudes of radiation quantities at the limit of CLAP validity may be within better than an order of magnitude agreement with the large separation limits. In that case we can make good estimates for the large separation case by taking the values at the CLAP limit.

An easy index for this limit has been suggested by Suen [24]. One can take the nonlinear initial data, extract perturbation quantities and compute Moncrief's two even parity gauge-invariant functions q_1 and q_2. For linearized data the linearized Hamiltonian constraint gives $q_2 = 0$, so the magnitude of q_2 is an indication of "how nonlinear" the initial data are, and therefore, presumably, how accurate linearized computations are for the evolution. In Figs. 8, and 9, we plot the value of q_2/q_1 as a function of radius. To make this nonlinearity index more plausible we have modified it in two ways. The factor of $(r/M-2)$ corrects for the divergence of q_2 at the horizon. If the mass ratio m_2/m_2 becomes very small, violations of sphericity must scale as m_2. We would then find that violations of nonlinearity were very small regardless how far apart the holes start, and regardless how badly the CLAP fails. To take into account the scaling of nonlinearities as m_2, we place a factor F in the denominator of the nonlinearity index. In the two figures we normalize separation with the ADM mass M, rather than with bare masses. Since the curves refer to a fixed set of masses, the ratio of M to m_1+m_2 is fixed.

The first figure shows the result for equal masses and ML initial geometry (see also [3]). In this case we know, from numerical relativity results, that the CLAP fails at around $L/M \sim 3-4$. The results in Fig. 8 show a dramatic increase in the hamiltonian violation as L/M increases beyond ~ 2 and this coincides, approximately, to the value of L/M for which CLAP starts to fail.

In Fig. 9 we show the equivalent results for ML holes with a ratio of Penrose mass $F = 0.1$; in the previous section we saw that ratios roughly around this value maximize the recoil velocity. The results in this figure suggest that at $L/M = 0.83$, CLAP must fail badly. We know, from the particle limit study [22] that CLAP estimates are quite accurate (within 20%) up to around $L/M \sim 1.5$ This implies that the CLAP method can work well even when there is significant "linearity violation" in the initial data. It also implies, unfortunately, that there may be no easy reliable way to esitmate the validity of CLAP calculations.

Let us now tentatively accept, from the particle limit results that for $F = 0.1$ the CLAP method is valid out to around $L/M \sim 1$, and that the energy and linear momentum at this limit are, to order of magnitude, as large as they would be for initially infinite separation (as in the case of equal mass holes). The plots in Figs. 6 and 7 then tell us that recoil velocities will always be well short of the several hundred km/sec values that would be astrophysically interesting.

FIG. 8. The linearized constraint violation for two equal mass ML holes, $F = 1$ according with Penrose, is shown for several values of initial separation. Here r^* is the coordinate $r + 2M \ln(r/2M - 1)$ for the Schwarzschild geometry.

FIG. 9. The linearized constraint violation for ML holes with a ratio $F = 0.1$ of the Penrose masses.

VI. CONCLUSIONS

The application of the CLAP method to collisions of unequal mass holes has provided one very tentative conclusion: The linear momentum generated in the collisions will be far too small to produce astrophysically interesting recoil velocity of the final hole.

The study has been much more successful in raising questions and in uncovering difficulties. The most important difficulty is the choice of the bare mass of the holes participating in a collision. It should be understood that this is not an issue specific to CLAP estimates. Rather, CLAP estimates were used to probe it. The general problem is: How do we best characterize an individual hole when it is interacting strongly with another gravitational source? And this issue is part of the broader question: How do we set up initial data to represent a black hole configuration?

Astrophysical models, or Newtonian physics applied to the early dynamics, can give us an initial configuration in terms of simple physical parameters (mass of the holes, separation,...). To turn this into appropriate initial data for numerical relativity we must know the correct general relativistic interpretation of the classical picture. This will be of crucial importance to the use of numerical relativity to study three dimensional black hole collisions. Codes to evolve black holes tend to be unstable. It is therefore important to apply the codes "at the last possible moment," i.e., only to follow the last orbit or last few orbits of black hole coalescence. It will be necessary then for those codes to begin with initial data for holes which are already interacting fairly strongly and it is in just this case that there is the most ambiguity in translating the Newtonian concept of the mass of a hole, into a parameter of the relativistic initial data.

We have considered three measures of bare mass. The "area-mass," and the "Lindquist mass" are well defined only for ML data, for which there are symmetric Einstein-Rosen bridges. The "Penrose" mass measure (though not generally applicable) can be computed for either ML or BL initial data (and in the latter case agrees with the obvious choice of bare mass in the asymptotically flat region of a throat). We have found very mixed messages about the physical meaningfulness of the various mass measures when the holes are initially close. One somewhat surprising message is that the area-mass and the Lindquist mass of each throat are numerically quite close. They are even closer if we make a more subtle comparison: the ratio of area/Lindquist masses of two holes, and the ratio of Penrose masses. This agreement is not a manifestation of some general necessity of all mass measures to agree. The Penrose mass and the area/Lindquist mass are markedly different for close separations.

The agreement of area-mass and Lindquist mass is unexpected, because they are based on such different criteria. The area-mass connects mass to the area of the minimum section of the Einstein-Rosen bridge, just as if it were an isolated Schwarzschild hole. It takes no direct account of the presence of a second throat. The Lindquist mass, by very sharp contrast, uses asymptotic masses of "images" used to form a single hole and subtracts an expression for binding energy due to gravitational interaction of the images. The binding energy is computed by Newtonian physics applied in the conformally flat space underlying the initial data. (Both the sum of asymptotic masses and the binding energy are divergent, but the sum is not.) It is often the case that when two very different ways of measuring a physical quantity agree it is taken as good evidence that the measurement is valid. This would suggest that we take seriously the area/Lindquist bare mass, perhaps for a wider class of problems. But the strange behavior seen in Fig. 4 for mass ratio $F = 0.75$ suggests even more strongly that this bare mass measure can be misleading.

ACKNOWLEDGMENTS

We would like to thank Carlos Lousto for many useful conversations, and also Madhavan Varadarajan for discussions of Penrose mass. We thank Carleton Detar for help with computational aspects of the work. ZA was supported by a PhD grant under PRAXIS XXI administered by JNICT (Portugal). This work was partially supported by NSF grant PHY-9507719.

APPENDIX A: THE BRILL-LINDQUIST SOLUTION FOR TWO BLACK HOLES

In this appendix we evaluate the coefficients γ_ℓ in the expansion (8) of the Brill-Lindquist solution (3).

When $|\vec{R}| > |\vec{R}_1|$ and $|\vec{R}| > |\vec{R}_2|$ the expansion of (3) in Legendre polynomials gives

$$\gamma_\ell = [(\frac{R_1}{M})^l \frac{\alpha_1}{M} + (\frac{R_2}{M})^l \frac{\alpha_2}{M}] \ . \tag{A1}$$

We can completely characterize the two holes by two parameters in the flat space: the "distance" $z_0 = |\vec{R}_2 - \vec{R}_1|$ and the "mass ratio" $C = \alpha_2/\alpha_1$. Choosing the origin of coordinates in this space at the ficticious center of mass, we can rewrite γ_ℓ as

$$\gamma_\ell = \frac{\alpha_1}{M}(\frac{z_0}{M})^l \frac{1}{(1+C)^l}[C^l + (-1)^l C] \ . \tag{A2}$$

where we chose the convention that hole 1 is on the positive z axis, hole 2 on the negative side and $0 < C \leq 1$. Since the total mass of the spacetime at the moment of time symmetry is

$$M = 2(\alpha_1 + \alpha_2) \ , \tag{A3}$$

i.e.,

$$\frac{\alpha_1}{M} = \frac{1}{2(1+C)} \ , \tag{A4}$$

we obtain

$$\gamma_\ell = (\frac{z_0}{M})^l \frac{1}{2(1+C)^{l+1}} [C^l + (-1)^l C] \ . \tag{A5}$$

The two parameters z_0 and C do not have a direct physical meaning. We therefore introduce the ratio of the bare masses of each black hole, $F = m_2/m_1$, and the separation between the apparent horizons, L, measured along the axis of symmetry and we express z_0 and C (and hence γ_l) in terms of them.

If we choose, for simplicity, the origin of coordinates to be at singularity 1,then L, the proper distance between apparent horizons is

$$L = \int_{z_1}^{z_2} [1 + \frac{1}{2(1+C)} (\frac{1}{z} + \frac{C}{z_0 - z})]^2 dz \ . \tag{A6}$$

Here z_1 and z_2 are the z-axis intersections of the apparent horizons surrounding holes 1 and 2, respectively. To find z_1, z_2 we numerically integrated the system of ODEs that determine all the extremal two dimensional surfaces of the BL solution (see [26] for details), and we searched along the segment of the z axis between the positions of the two holes (i.e. between $z = 0$ and $z = z_0$) for the critical values z_1 and z_2 at which the extremal surfaces are closed. The bare masses of hole 1 and hole 2 are [13]:

$$m_1 = 2\alpha_1 (1 + \frac{\alpha_2}{z_0}) \tag{A7}$$

$$m_2 = 2\alpha_2 (1 + \frac{\alpha_1}{z_0}) \ , \tag{A8}$$

and hence

$$F = \frac{m_2}{m_1} = \frac{1 + \frac{1}{2(1+C)} \frac{M}{z_0}}{1 + \frac{C}{2(1+C)} \frac{M}{z_0}} C \ . \tag{A9}$$

Solving for C in terms of F and z_0 we obtain

$$C = \frac{(F-1)(2 + \frac{M}{z_0}) + \sqrt{(1-F)^2 (2 + \frac{M}{z_0})^2 + 16F}}{4} \ . \tag{A10}$$

Typically to characterize a BL solution, we choose an F and a set of z_0 values. Then from (A10) we obtain the corresponding set of C values and from (A6) the L value corresponding to each pair (C, z_0).

APPENDIX B: THE MISNER-LINDQUIST SOLUTION FOR TWO BLACK HOLES

In this appendix we present the ML solution and some additional details relevant to the CLAP of this solution. We will follow closely Lindquist [16] who derived such a solution in implicit form. Our notation is also the same as his with minor changes.

1. The solution

The conformal factor can be written in the explicit form (4)

$$\Phi = 1 + \sum_{n=1}^{\infty}(\frac{a_n}{|\vec{x} - \vec{d_n}|} + \frac{b_n}{|\vec{x} - \vec{e_n}|}) \tag{B1}$$

Where $\vec{d_1}$ is the position of sphere 1, of radius a and $\vec{e_1}$ the position of sphere 2, of radius b, relative to a given origin in the flat space (the spheres in the flat space correspond to the throats in the three geometry) and $\vec{d_n}$ are the positions of the image poles of $\vec{d_1}$, $\vec{e_n}$ are the positions of the image poles of $\vec{e_1}$ with a_n and b_n being the corresponding weights. These coefficients obey the recursion relations

- **If n is even**

$$\begin{aligned} d_n &= e_1 - \frac{b^2}{e_1 + d_{n-1}} \\ a_n &= \frac{b}{e_1 + d_{n-1}} a_{n-1} \\ e_n &= d_1 - \frac{a^2}{d_1 + e_{n-1}} \\ b_n &= \frac{a}{d_1 + e_{n-1}} b_{n-1} \end{aligned}$$

- **If n is odd** ($n \geq 3$)

$$\begin{aligned} d_n &= d_1 - \frac{a^2}{d_1 + d_{n-1}} \\ a_1 &= a \\ a_n &= \frac{a}{d_1 + d_{n-1}} a_{n-1} \\ e_n &= e_1 - \frac{b^2}{e_1 + e_{n-1}} \\ b_1 &= b \\ b_n &= \frac{b}{e_1 + e_{n-1}} b_{n-1} \end{aligned}$$

whose solution is (see for example Smythe [25])

- **If n is even**

$$d_n = e_1 - c(1 - \frac{ba \sinh(n+2)\mu_0 + a^2 \sinh n\mu_0}{c^2 \sinh n\mu_0}) \tag{B2a}$$

$$a_n = \frac{ab \sinh 2\mu_0}{c \sinh n\mu_0} \tag{B2b}$$

$$e_n = d_1 - c(1 - \frac{ba \sinh(n+2)\mu_0 + b^2 \sinh n\mu_0}{c^2 \sinh n\mu_0}) \tag{B2c}$$

$$b_n = \frac{ab \sinh 2\mu_0}{c \sinh n\mu_0} \tag{B2d}$$

- **If n is odd**

$$d_n = d_1 - c(1 - \frac{\sinh(n+1)\mu_0}{\sinh(n+1)\mu_0 + \frac{a}{b} \sinh(n-1)\mu_0}) \tag{B3a}$$

$$a_n = \frac{ab\sinh 2\mu_0}{b\sinh(n+1)\mu_0 + a\sinh(n-1)\mu_0} \tag{B3b}$$

$$e_n = e_1 - c(1 - \frac{\sinh(n+1)\mu_0}{\sinh(n+1)\mu_0 + \frac{b}{a}\sinh(n-1)\mu_0}) \tag{B3c}$$

$$b_n = \frac{ab\sinh 2\mu_0}{a\sinh(n+1)\mu_0 + b\sinh(n-1)\mu_0} \tag{B3d}$$

where c is the distance (in the flat space) between the centers of the two spheres

$$c = d_1 + e_1 \tag{B4}$$

and μ_0 is given by

$$\cosh 2\mu_0 = \frac{c^2 - a^2 - b^2}{2ab} \ . \tag{B5}$$

2. The choice of parameters

In the background three dimensional Euclidean space there are two natural dimensionless parameters: the ratio $C = b/a$ of the radii a and b of the spheres 1 and 2, and the ratio of the distance between the two throats (i.e. the distance between the centers of the spheres $c = d_1 + e_1$) to the radius of one of the throats say a: $D = c/a$. We will always restrict attention to the cases $0 < C \leq 1$ i.e. hole 1 on the positive z axis is greater or equal to hole 2 on the negative z axis. We must also have $D > 1 + C$ and from (B 1)

$$\mu_0 = \frac{1}{2}\cosh^{-1}[\frac{D^2 - 1 - C^2}{2C}] \tag{B6}$$

These two parameters, like C and z_0/M in the BL solution, completely characterize the Misner-Lindquist solution. As in the BL solution, however, they do not have a direct physical meaning and we must look to other way of parameterizing the ML solution. One parameter which can be defined in a natural way in the ML solution, the distance between the two holes defined by the length of the geodesic which threads through their corresponding Einstein-Rosen bridges, L, is discussed in the first part of this section. Another physical parameter is the ratio between the "bare" masses of each ML hole, $F = m_2/m_1$. As discussed above, we lack a unique, well defined, notion of bare mass of each hole. The Lindquist masses presented on the second part are just a possibility. Once we have a prescription that gives the masses we can parametrize the ML solution either by F and L/M or by F and $L/(m_1+m_2)$.

Due to the difficulty of obtaining C and D as functions of these physical parameters, we will instead derive all the quantities in terms of C and D.

As we will see the restriction $D > 1 + C$, equivalent to $\mu_0 > 0$, is required in order to obtain convergence of the different series which appear in the next sections.

a. Invariant distance of separation

Instead of using the distance between the throats (i.e. the parameter D defined above) as measured in the Euclidean space, it makes more sense physically to use the invariant separation distance between the two holes defined as the length of the shortest closed path which threads through their corresponding E-R bridges. Such a curve is a geodesic of the initial slice. To evaluate its length it is convenient to work in bispherical coordinates instead of cartesian ones.

In these coordinates the metric of the initial surface is

$$ds^2 = \Phi^4(\frac{f}{\cosh\mu - \cos\eta})^2[d\mu^2 + d\eta^2 + \sin^2\eta d\varphi^2] \ . \tag{B7}$$

We introduce

$$a = f\,\mathrm{csch}\,\mu_1 \tag{B8a}$$

$$d_1 = f\coth\mu_1 \tag{B8b}$$

$$b = f\,\mathrm{csch}\,\mu_2 \tag{B8c}$$

$$e_1 = f\coth\mu_2 \tag{B8d}$$

where

$$\mu_1 + \mu_2 = 2\mu_0 \tag{B9}$$

$$\mu_2 = \sinh^{-1} \frac{\sinh 2\mu_0}{D} \tag{B10}$$

$$f = b \sinh \mu_2 \ . \tag{B11}$$

Substituting (B8) in (B2) and (B3) we obtain a convenient form for the coefficients of Φ in (B1). (Compare with (4.7) in Lindquist [16] when the two black holes are equal.)

- **If n is even**

$$a_n = b_n = f \operatorname{csch} n\mu_0 \tag{B12a}$$

$$d_n = e_n = f \coth n\mu_0 \tag{B12b}$$

- **If n is odd**

$$a_n = f \operatorname{csch} [(n+1)\mu_0 - \mu_2] \tag{B13a}$$

$$b_n = f \operatorname{csch} [(n-1)\mu_0 + \mu_2] \tag{B13b}$$

$$d_n = f \coth[(n+1)\mu_0 - \mu_2] \tag{B13c}$$

$$e_n = f \coth[(n-1)\mu_0 + \mu_2] \ . \tag{B13d}$$

and the conformal factor becomes

$$\Phi = \sum_{n=-\infty}^{\infty} \frac{1}{\sqrt{\cosh(\mu + 4n\mu_0) - \cos\eta}} + \frac{1}{\sqrt{\cosh[\mu + 4n\mu_0 + 2\mu_2] - \cos\eta}} (\cosh\mu - \cos\eta)^{\frac{1}{2}} \tag{B14}$$

which converges if and only if $\mu_0 > 0$.

We note that this parametrization implies a specific choice of origin in the Euclidean space, however the geodesic distance between the two throats is the same independent of the choice of origin. It is thus just a matter of convenience. The equations of the throats $x^2 + y^2 + (z - d_1)^2 = a^2$ and $x^2 + y^2 + (z + e_1)^2 = b^2$ become $\mu = \mu_1$ and $\mu = -\mu_2$ respectively.

The geodesic of interest is $\varphi = 0$, $\eta = \pi$. Therefore the distance of separation between the holes is

$$L = \int_{-\mu_2}^{\mu_1} \sqrt{g_{\mu\mu}(\mu, \pi)} d\mu = f \int_{-\mu_2}^{\mu_1} \Phi^2(\mu, \pi) \frac{1}{\cosh\mu + 1} d\mu \ . \tag{B15}$$

or explicitly

$$L = 2f \left\{ 1 + \frac{\mu_2}{\sinh(\mu_2)} + \sum_{n=1}^{\infty} [\frac{4n\mu_0}{\sinh(2n\mu_0)} + \frac{2n\mu_0 - \mu_2}{\sinh(2n\mu_0 - \mu_2)} + \frac{2n\mu_0 + \mu_2}{\sinh(2n\mu_0 + \mu_2)}] \right\} \tag{B16}$$

Again this series converges if and only if $\mu_0 > 0$.

b. The Lindquist mass

The bare masses of the holes, according to Lindquist [16], are

$$m_1 = 2\sum_{n=1}^{\infty}[a_{2n-1} + b_{2n} + \sum_{m=1}^{\infty}\frac{a_{2n-1}a_{2m}}{|\vec{d}_{2n-1} - \vec{d}_{2m}|} + \frac{a_{2n-1}b_{2m-1}}{|\vec{d}_{2n-1} - \vec{e}_{2m-1}|} + \frac{b_{2n}a_{2m}}{|\vec{e}_{2n} - \vec{d}_{2m}|} + \frac{b_{2n}b_{2m-1}}{|\vec{e}_{2n} - \vec{e}_{2m-1}|}] \tag{B17}$$

$$m_2 = 2\sum_{n=1}^{\infty}[a_{2n} + b_{2n-1} + \sum_{m=1}^{\infty}\frac{a_{2n}a_{2m-1}}{|\vec{d}_{2n} - \vec{d}_{2m-1}|} + \frac{a_{2n}b_{2m}}{|\vec{d}_{2n} - \vec{e}_{2m}|} + \frac{b_{2n-1}a_{2m-1}}{|\vec{e}_{2n-1} - \vec{d}_{2m-1}|} + \frac{b_{2n-1}b_{2m}}{|\vec{e}_{2n-1} - \vec{e}_{2m}|}] \ . \tag{B18}$$

which using the coefficients in (B12) and (B13) become

$$m_1 = 2f\sum_{n=1}^{\infty} n\{\frac{2}{\sinh 2n\mu_0} + \frac{1}{\sinh(2n\mu_0 - \mu_2)} + \frac{1}{\sinh(2n\mu_0 + \mu_2)}\} \tag{B19}$$

$$m_2 = 2f\sum_{n=1}^{\infty} n\{\frac{2}{\sinh 2n\mu_0} + \frac{1}{\sinh[2(n+1)\mu_0 - \mu_2]} + \frac{1}{\sinh[2(n-1)\mu_0 + \mu_2]}\} \tag{B20}$$

Both series converge if and only if $\mu_0 > 0$.

3. The choice of origin

In order to determine the energy and the recoil velocity we need to choose the origin in such a way that the dipole term in (8) vanishes. This requires that the origin be located at the "center of mass" (CM) of the "masses" a_n, b_n,

$$\sum_{n=1}^{\infty} a_n\vec{d}_{nCM} + b_n\vec{e}_{nCM} = 0 \ . \tag{B21}$$

(The a_n and b_n do not depend on the choice of origin). One systematic way of determining the $\vec{d}_{nCM}$, $\vec{e}_{nCM}$ is the following

- We choose an arbitrary origin, for example the one for which bispherical coordinates can be introduced and pick the corresponding d_n and e_n in (B12) and (B13).
- We next find the center of mass position using

$$z_{CM} = \frac{\sum_{n=1} -a_{2n}d_{2n} + a_{2n-1}d_{2n-1} + b_{2n}e_{2n} - b_{2n-1}e_{2n-1}}{\sum_{n=1} a_n + b_n} \ . \tag{B22}$$

- Finally we determine the position of a given image relatively to the CM, using the formula

$$\vec{z}_{iCM} = \vec{z}_i - \vec{z}_{CM} \tag{B23}$$

or in scalar form

$$d_{2nCM} = -d_{2n} - z_{CM} \tag{B24a}$$
$$e_{2n+1CM} = -e_{2n+1} - z_{CM} \tag{B24b}$$
$$e_{2nCM} = e_{2n} - z_{CM} \tag{B24c}$$
$$d_{2n+1CM} = d_{2n+1} - z_{CM} \tag{B24d}$$

4. The γ_ℓ coefficients

Comparing (4) with (8), we obtain the coefficients γ_ℓ

$$\gamma_\ell = \sum_{n=1}^{\infty} [\frac{a_n}{M}(\frac{d_{nCM}}{M})^\ell + \frac{b_n}{M}(\frac{e_{nCM}}{M})^\ell] \ . \tag{B25}$$

5. The mass of the system

To determine the γ_ℓ above we need to know a dimensionless parameter, say the radius of sphere 2, b, per unit of mass. This can easily be done by expressing the mass in terms of the coefficients in the conformal factor. The ADM mass of the spacetime at the moment of time symmetry is the coefficient of $1/r$ in an expansion of ds^2 in inverse powers of r. The result is

$$M = 2\sum_{n=1} a_n + b_n \ . \tag{B26}$$

If the explicit expressions in (B2) and (B3) are used, this becomes

$$M = 2f\sum_{n=1}^{\infty}\{\frac{2}{\sinh 2n\mu_0} + \frac{1}{\sinh(2n\mu_0 - \mu_2)} + \frac{1}{\sinh[2(n-1)\mu_0 + \mu_2]}\} \tag{B27}$$

from which we can express b in terms of C and D. We note that once more the series converges if and only if $\mu_0 > 0$.

APPENDIX C: THE PENROSE QUASI-LOCAL MASS OF ONE ML BLACK HOLE

In Penrose's approach a complex quantity $A_{\alpha\beta}$, the momentum-angular momentum twistor of the source inside a 2-surface S (*with topology* S^2) is defined and the total mass threading through S is [17]

$$m_P^2 = -\tfrac{1}{2}A_{\alpha\beta}\overline{A}^{\alpha\beta} \ . \tag{C1}$$

Certain problems with this definition remain. In order to evaluate this mass we need a Hermitian "norm" defined for the surface S as a whole. This norm can only be defined unambiguosly if S can be embedded in some conformally flat space-time in such a way that both its intrinsic geometry (induced metric) and the quantities characterizing its extrinsic curvature are unaltered from their values when S is embedded in the true spacetime. However this is not a difficulty for the ML solution (and BL solution), since any time symmetric *conformally flat* hypersurface can be embedded in a conformally flat 4-space as a surface of constant t with the same intrinsic and extrinsic geometries and hence also all 2-surfaces lying on this hypersurface.

In fact Tod [18] has evaluated the Penrose quasi-local mass associated with a 2-surface S obeying the restriction above, including the time symmetric case. He showed that in the BL case, the Penrose mass of each hole coincides with the ADM mass and that for both BL and ML solutions the total Penrose mass of the spacetime at the instant of time symmetry is the same as the total ADM mass. He also derived the mass of each ML hole, when the masses are equal.

In this appendix we use Tod's results to derive the Penrose mass of each ML black hole when their masses are unequal. We will use a signature $(+---)$.

Let $\mathbf{t}$ denote the unit timelike vector normal to the time symmetric 3-surface Σ. The Penrose mass "enclosed" by the two surface S lying in Σ with normal $\mathbf{n}$ is

$$m_P^2 = P_a\overline{P}^a - \tfrac{1}{2}\overline{\lambda}^{AB}\mu_{AB} - \tfrac{1}{2}\lambda^{A'B'}\overline{\mu}_{A'B'} \tag{C2}$$

which we can rewrite in terms of spinors as (see Tod [18]))

$$m_P^2 = -2t_{A'(B}P_{A)}^{A'}t^{C'(B}\overline{P}_{C'}^{A)} + P^b t_b\overline{(P^b t_b)} + \overline{\lambda}^{AB}t_B^{A'}t_{A'}^{C}\mu_{AC} + \lambda^{A'B'}t_{B'}^{A}t_A^{C'}\overline{\mu}_{A'B'} \tag{C3}$$

where

$$\mu_{AB}t_{A'}^{B} = \frac{-i}{2\pi}\int\{2(\vec{n}.\nabla\Phi)\nabla\Phi - (\nabla\Phi)^2\vec{n}\}dS \tag{C4}$$

$$t^a P_a = \frac{1}{2\pi}\int\{-\Phi\vec{n}.\nabla\Phi - 2(\vec{n}.\nabla\Phi)(\vec{R}.\nabla\Phi) + (\nabla\Phi)^2(\vec{n}.\vec{R})\}dS \tag{C5}$$

$$t_{A'(B}P_{A)}^{A'} = \frac{1}{2\pi}\int\{\Phi(\nabla\Phi\times\vec{n}) + (\nabla\Phi)^2\vec{n}\times\vec{R} - 2(\nabla\Phi.\vec{n})(\nabla\Phi\times\vec{R})\}dS \tag{C6}$$

$$t_{B'}^{A}\lambda^{A'B'} = \frac{i}{2\pi}\int\{\vec{n}(\frac{1}{2}\Phi^2 + \Phi(\vec{R}.\nabla\Phi) + \frac{1}{2}R^2(\nabla\Phi)^2) + \vec{R}(2(\vec{n}.\nabla\Phi)(\vec{R}.\nabla\Phi) - (\vec{n}.\vec{R})(\nabla\Phi)^2 + \Phi\vec{n}.\nabla\Phi) - \nabla\Phi(\Phi(\vec{n}.\vec{R}) + R^2(\vec{n}.\nabla\Phi)\}dS \tag{C7}$$

with all expressions on the right hand side written in terms of a three vector notation on flat three-space. To evaluate the integrals we transform them to integrals over a volume spanned by S

$$\mu_{AB}t_{A'}^{B} = -\frac{i}{\pi}\int\nabla\Phi\nabla^2\Phi d^3x \tag{C8}$$

$$t^a P_a = -\frac{1}{2\pi}\int(\Phi + 2\vec{R}.\nabla\Phi)\nabla^2\Phi d^3x \tag{C9}$$

$$t_{A'(B}P_{A)}^{A'} = \frac{1}{\pi}\int(\vec{R}\times\nabla\Phi)\nabla^2\Phi d^3x \tag{C10}$$

$$t_{B'}^{A}\lambda^{A'B'} = \frac{i}{2\pi}\int[2\vec{R}.\nabla\Phi\vec{R} + \Phi\vec{R} - R^2\nabla\Phi]\nabla^2\Phi d^3x\ . \tag{C11}$$

In the ML solution the conformal factor (4) leads to

$$\nabla\Phi = \sum_{n=1}^{\infty} a_n\frac{\vec{d_n} - \vec{R}}{|\vec{R} - \vec{d_n}|^3} + b_n\frac{\vec{e_n} - \vec{R}}{|\vec{R} - \vec{e_n}|^3} \tag{C12}$$

and

$$\nabla^2\Phi = -4\pi[\sum_{n=1}^{\infty} a_n\delta(\vec{R} - \vec{d_n}) + \sum_{n=1}^{\infty} b_n\delta(\vec{R} - \vec{e_n})]\ . \tag{C13}$$

In order to evaluate the Penrose mass of the hole 1, we choose the 2-surface to be the sphere with center at $\vec{R} = \vec{d_1}$ (the throat of radius a). Remembering that all the images located at $\vec{R} = \vec{d}_{2n-1}$ and $\vec{R} = \vec{e}_{2n}$ lie inside that sphere we obtain

$$(\mu_{AB}t^B_{A'})_1 = 4i\sum_{i=1}^{\infty}\sum_{n=1}^{\infty} a_{2i-1}(a_{2n}\frac{\vec{d}_{2n}-\vec{d}_{2i-1}}{|\vec{d}_{2n}-\vec{d}_{2i-1}|^3} + b_{2n-1}\frac{\vec{e}_{2n-1}-\vec{d}_{2i-1}}{|\vec{e}_{2n-1}-\vec{d}_{2i-1}|^3}) +$$
$$4i\sum_{i=1}^{\infty}\sum_{n=1}^{\infty} b_{2i}(b_{2n-1}\frac{\vec{e}_{2n-1}-\vec{e}_{2i}}{|\vec{e}_{2n-1}-\vec{e}_{2i}|^3} + a_{2n}\frac{\vec{d}_{2n}-\vec{e}_{2i}}{|\vec{d}_{2n}-\vec{e}_{2i}|^3})$$

$$(t^aP_a)_1 = 2\sum_{i=1}^{\infty} a_{2i-1} + b_{2i} + 2\sum_{i=1}^{\infty}\sum_{n=1}^{\infty} a_{2i-1}[a_{2n}\frac{d^2_{2n}-d^2_{2i-1}}{|\vec{d}_{2i-1}-\vec{d}_{2n}|^3}$$
$$+b_{2n-1}\frac{e^2_{2n-1}-d^2_{2i-1}}{|\vec{d}_{2i-1}-\vec{e}_{2n-1}|^3}] + 2\sum_{i=1}^{\infty}\sum_{n=1}^{\infty} b_{2i}[b_{2n-1}\frac{e^2_{2n-1}-e^2_{2i}}{|\vec{e}_{2i}-\vec{e}_{2n-1}|^3} + a_{2n}\frac{d^2_{2n}-e^2_{2i}}{|\vec{e}_{2i}-\vec{d}_{2n}|^3}]$$

$$[t_{A'(B}P^{A'}_{A)}]_1 = 0$$

since all images lie along the z axis, and

$$(t^A_{B'}\lambda^{A'B'})_1 = -2i\sum_{i=1}^{\infty} a_{2i-1}\vec{d}_{2i-1} + b_{2i}\vec{e}_{2i} - 2i\sum_{i=1}^{\infty}\sum_{n=1}^{\infty} a_{2i-1}[a_{2n}\frac{d^2_{2n}\vec{d}_{2i-1}-d^2_{2i-1}\vec{d}_{2n}}{|\vec{d}_{2i-1}-\vec{d}_{2n}|^3}$$
$$+b_{2n-1}\frac{e^2_{2n-1}\vec{d}_{2i-1}-d^2_{2i-1}\vec{e}_{2n-1}}{|\vec{d}_{2i-1}-\vec{e}_{2n-1}|^3}] - 2i\sum_{i=1}^{\infty}\sum_{n=1}^{\infty} b_{2i}[b_{2n-1}\frac{e^2_{2n-1}\vec{e}_{2i}-e^2_{2i}\vec{e}_{2n-1}}{|\vec{e}_{2i}-\vec{e}_{2n-1}|^3}$$
$$+a_{2n}\frac{d^2_{2n}\vec{e}_{2i}-e^2_{2i}\vec{d}_{2n}}{|\vec{e}_{2i}-\vec{d}_{2n}|^3}]$$

and the Penrose quasi-local mass of black hole 1 will be

$$m^2_{1P} = [(P_at^a)_1]^2 + 2(\overline{\lambda}^{AB}t^{A'}_B)_1(t^C_{A'}\mu_{AC})_1 \ . \tag{C14}$$

Similarly if we take for volume of integration the sphere of radius b we get

$$(\mu_{AB}t^B_{A'})_2 = -(\mu_{AB}t^B_{A'})_1$$

$$(t^aP_a)_2 = 2\sum_{i=1}^{\infty} a_{2i} + b_{2i-1} - 2\sum_{i=1}^{\infty}\sum_{n=1}^{\infty} a_{2i-1}[a_{2n}\frac{d^2_{2n}-d^2_{2i-1}}{|\vec{d}_{2i-1}-\vec{d}_{2n}|^3}$$
$$+b_{2n-1}\frac{e^2_{2n-1}-d^2_{2i-1}}{|\vec{d}_{2i-1}-\vec{e}_{2n-1}|^3}] - 2\sum_{i=1}^{\infty}\sum_{n=1}^{\infty} b_{2i}[b_{2n-1}\frac{e^2_{2n-1}-e^2_{2i}}{|\vec{e}_{2i}-\vec{e}_{2n-1}|^3} + a_{2n}\frac{d^2_{2n}-e^2_{2i}}{|\vec{e}_{2i}-\vec{d}_{2n}|^3}]$$

$$[t_{A'(B}P^{A'}_{A)}]_2 = 0$$

$$(t^A_{B'}\lambda^{A'B'})_2 = -2i\sum_{i=1}^{\infty} a_{2i}\vec{d}_{2i} + b_{2i-1}\vec{e}_{2i-1} + 2i\sum_{i=1}^{\infty}\sum_{n=1}^{\infty} a_{2i-1}[a_{2n}\frac{d^2_{2n}\vec{d}_{2i-1}-d^2_{2i-1}\vec{d}_{2n}}{|\vec{d}_{2i-1}-\vec{d}_{2n}|^3}$$
$$+b_{2n-1}\frac{e^2_{2n-1}\vec{d}_{2i-1}-d^2_{2i-1}\vec{e}_{2n-1}}{|\vec{d}_{2i-1}-\vec{e}_{2n-1}|^3}] + 2i\sum_{i=1}^{\infty}\sum_{n=1}^{\infty} b_{2i}[b_{2n-1}\frac{e^2_{2n-1}\vec{e}_{2i}-e^2_{2i}\vec{e}_{2n-1}}{|\vec{e}_{2i}-\vec{e}_{2n-1}|^3}$$
$$+a_{2n}\frac{d^2_{2n}\vec{e}_{2i}-e^2_{2i}\vec{d}_{2n}}{|\vec{e}_{2i}-\vec{d}_{2n}|^3}]$$

and the corresponding Penrose mass will be

$$m^2_{2P} = [(P_at^a)_2]^2 + 2(\overline{\lambda}^{AB}t^{A'}_B)_2(t^C_{A'}\mu_{AC})_2 \ . \tag{C15}$$

To compute the total mass at the instant of time symmetry we choose for surface of integration a 2-sphere surrounding both throats. Then each term above add up and we get

$$(\mu_{AB}t^B_{A'})_T = (\mu_{AB}t^B_{A'})_1 + (\mu_{AB}t^B_{A'})_2 = 0$$

$$(t^a P_a)_T = (t^a P_a)_1 + (t^a P_a)_2 = 2\sum_{i=1}^{\infty} a_i + b_i$$

$$[t_{A'(B}P^{A'}_{A)}]_T = (t_{A'(B}P^{A'}_{A)})_1 + (t_{A'(B}P^{A'}_{A)})_2 = 0$$

and

$$(t^A_{B'}\lambda^{A'B'})_T = -2i\sum_{i=1}^{\infty}(a_i\vec{d}_i + b_i\vec{e}_i)$$

and hence

$$M = 2\sum_{i=1}^{\infty} a_i + b_i \tag{C16}$$

which coincides with the ADM mass (appendix B, expression (B26)). As expected, this mass is not equal to the sum of the two individual masses. The difference is the binding energy

$$E_B = M - m_{1P} - m_{2P}\ . \tag{C17}$$

In the special case in which the holes have equal mass, we obtain

$$(t^a P_a)_1 = (t^a P_a)_2 = \tfrac{1}{2}M \tag{C18}$$

$$(\mu_{AB}t^B_{A'})_1 = -(\mu_{AB}t^B_{A'})_2 = -iI = -4i\sum_{n=1}^{\infty}\sum_{m=1}^{\infty}\frac{\sinh n\mu_0 \sinh m\mu_0}{\sinh^2(n+m)\mu_0} \tag{C19}$$

$$(t^A_{B'}\lambda^{A'B'})_1 = -(t^A_{B'}\lambda^{A'B'})_2 = -iJ = -2ia^2\sinh\mu_0(\sum_{n=1}^{\infty}\frac{\cosh n\mu_0}{\sinh^2 n\mu_0}$$
$$+\sum_{n=1}^{\infty}\sum_{m=1}^{\infty}\frac{\cosh n\mu_0\cosh m\mu_0}{\sinh^2(m+n)\mu_0})$$

giving

$$m^2_{1P} = m^2_{2P} = \tfrac{1}{4}M^2 + 2IJ \tag{C20}$$

a result obtained by Tod [18].

---

[1] A. A. Abramovici *et al.*, Science **256**, 325 (1992); K. S. Thorne, submitted to *Proceedings of Snowmass 94 Summer Study on Particle and Nuclear Astrophysics and Cosmology*, eds. W. W. Kolb and R. Peccei (World Scientific, Singapore).

[2] Proceedings of the November 1994 meeting of the Grand Challenge Alliance to study black hole collisions may be obtained by contacting E. Seidel at NCSA (unpublished).

[3] A. Abrahams and R. H. Price, Phys. Rev. **D53**, 1963 (1996).

[4] R. H. Price and J. Pullin, Phys. Rev. Lett. **72**, 3297 (1994).

[5] P. Anninos, R. H. Price, J. Pullin, E. Seidel and W.-M. Suen, Phys. Rev. D **52**, 4462 (1995).
[6] A. Abrahams and R. H. Price, Phys. Rev. **D53**, 1972 (1996).
[7] A. M. Abrahams and G. B. Cook, Phys. Rev. D **50**, R2364 (1994).
[8] J. Baker, A. Abrahams, P. Anninos, S. Brandt, R. H. Price, J. Pullin, E. Seidel, preprint gr-qc/9608064 (1996) .
[9] H.-P. Nollert, private communication.
[10] R. Gleiser, C. O. Nicasio, R. H. Price, and J. Pullin, Class. Quantum Grav. **13** L117 (1996).
[11] R. Gleiser, C. O. Nicasio, R. H. Price, and J. Pullin, to appear in Phys. Rev. Lett.
[12] J. Bowen and J. W. York, Jr., Phys. Rev. **D21**, 2047 (1980).
[13] D. R. Brill and R. W. Lindquist, Phys. Rev. **131**, 471 (1964).
[14] C. Misner, Ann. Phys. (N.Y.) **24**, 102 (1963).
[15] C. Misner, Phys. Rev. **118**, 1110 (1960).
[16] R. W. Lindquist, J. Math. Phys., **4**, 938 (1963).
[17] R. Penrose, Proc. R. Soc. Lond. **A 381**, 53 (1982).
[18] K. P. Tod, Proc. R. Soc. Lond. **A 388**, 457 (1983).
[19] R. Penrose, in *Global Riemannian Geometry*, edited by T. J. Willmore and N. Hitchin (Ellis Horwood Limited, Chichester, England, 1984), p. 203.
[20] V. Moncrief, Ann. Phys. (NY) **88**, 323 (1974).
[21] F. Zerilli, Phys. Rev. Lett. **24** 737, (1971).
[22] C. O. Lousto and R. H. Price, preprint gr-qc/9609012(1996).
[23] V. Moncrief, Ap. J. **238**, 333 (1980).
[24] W.-M. Suen, private communication.
[25] William R. Smythe, *Static and dynamic electricity* (McGraw Hill, New York, 1968).
[26] N. T. Bishop, Gen. Rel. Grav. **16**, 589 (1984).

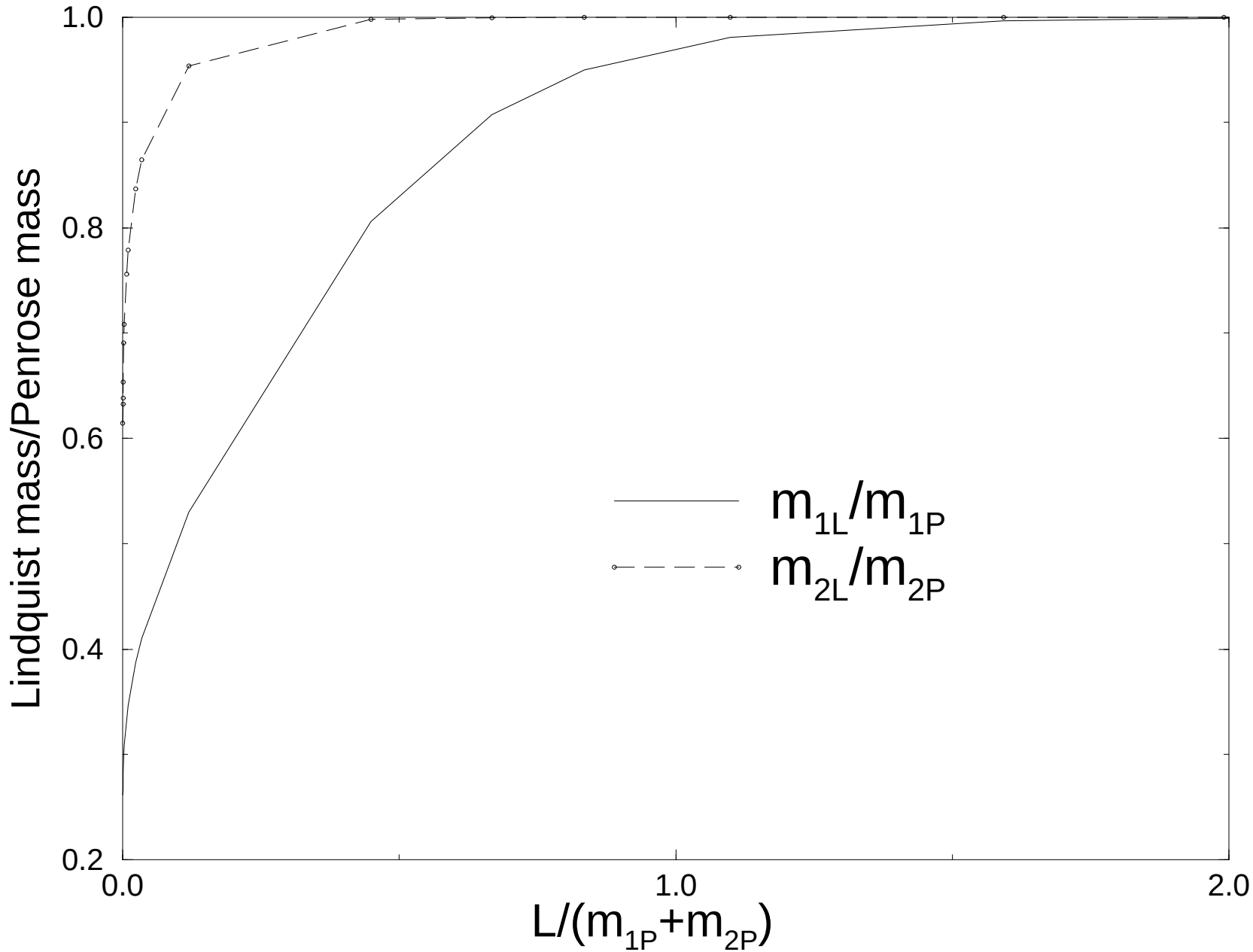
1.0
0.8
0.6
0.4
0.2
0.0
1.0
2.0
Lindquist mass/Penrose mass
L/(m1P+m2P)
m1L/m1P
m2L/m2P

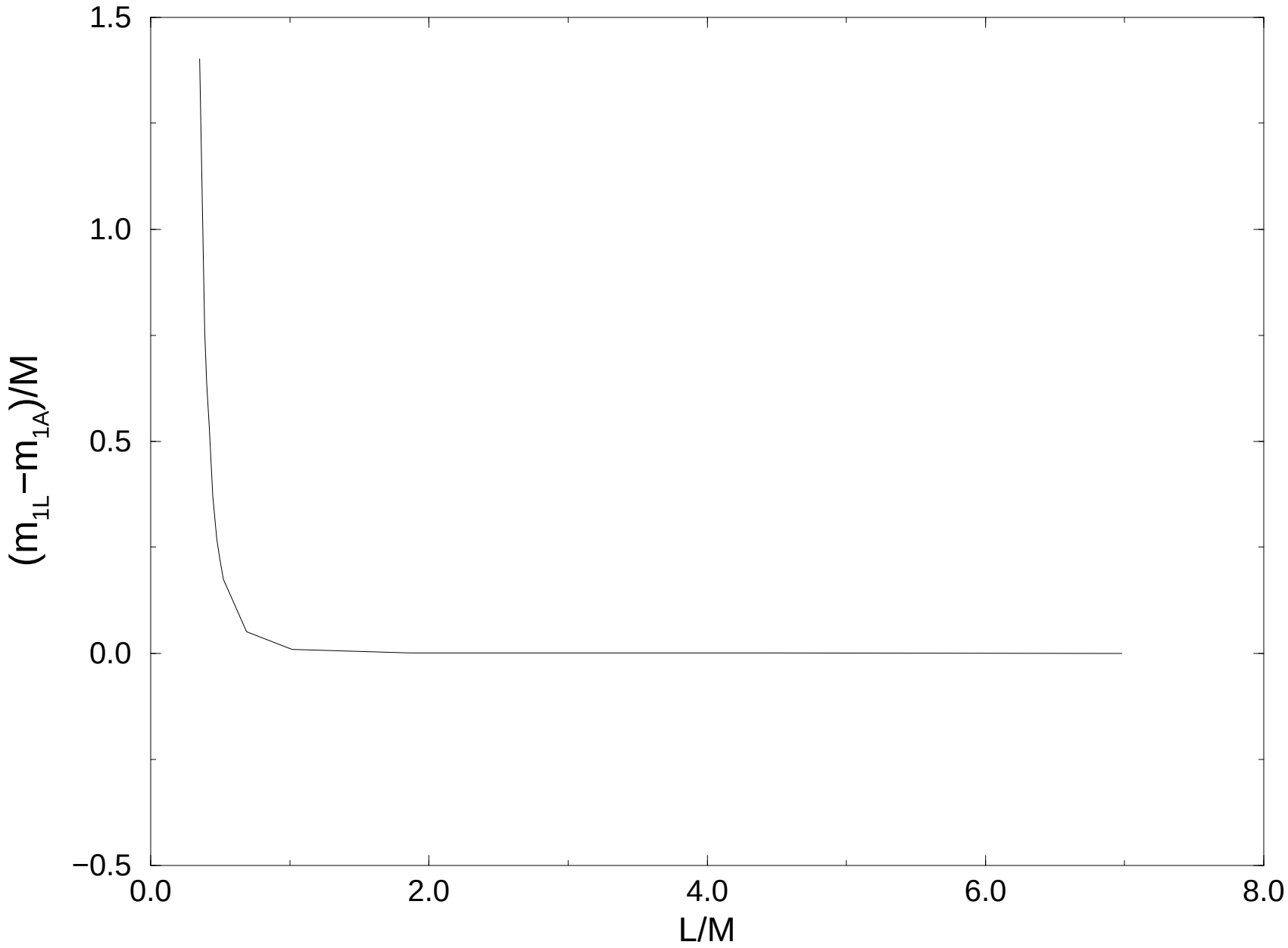
1.5
1.0
0.5
0.0
−0.5
0.0
2.0
4.0
6.0
8.0
L/M
(m1L−m1A)/M

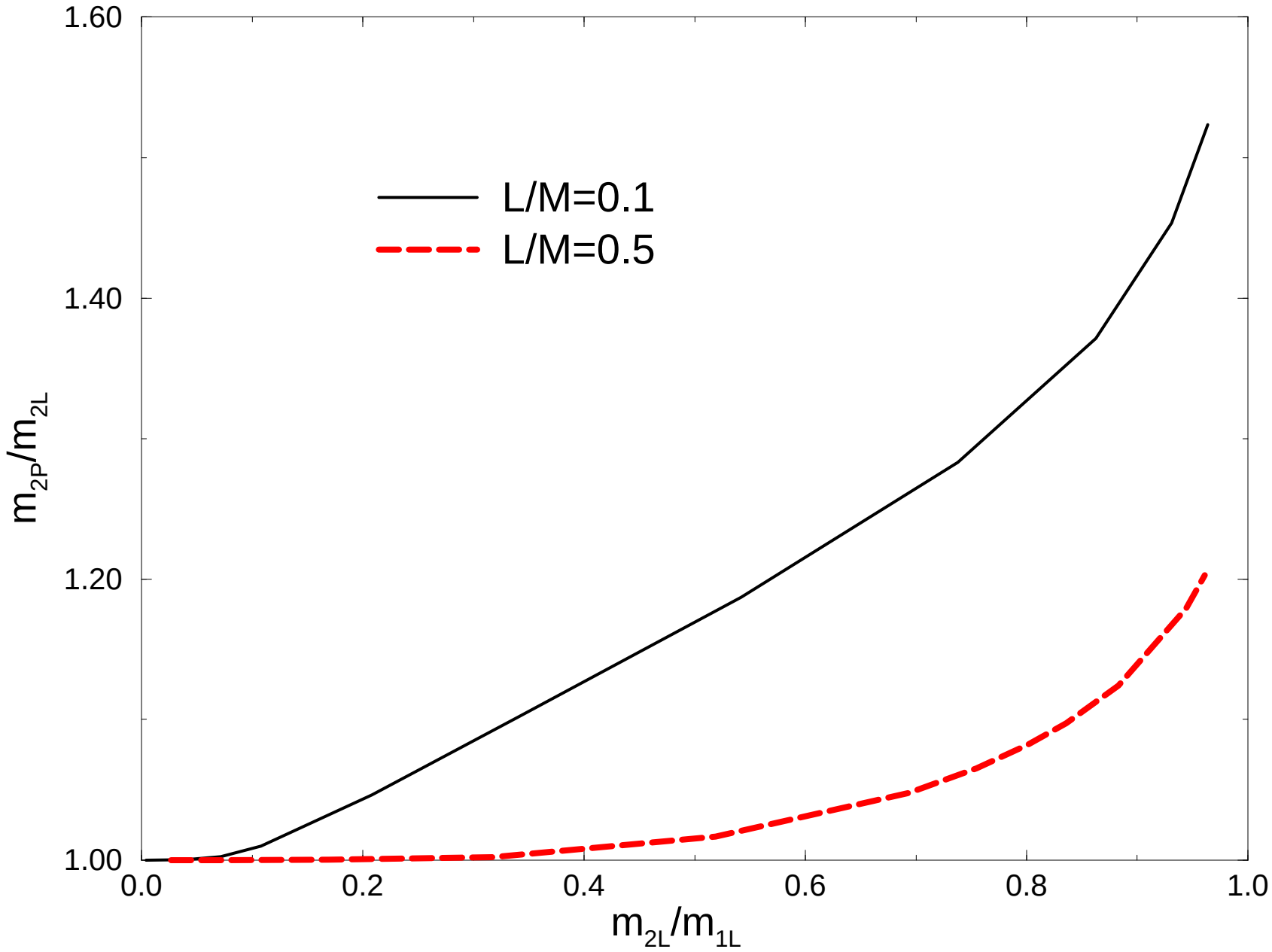
1.60
1.40
1.20
1.00
0.0
0.2
0.4
0.6
0.8
1.0
L/M=0.1
L/M=0.5
m2P/m2L
m2L/m1L

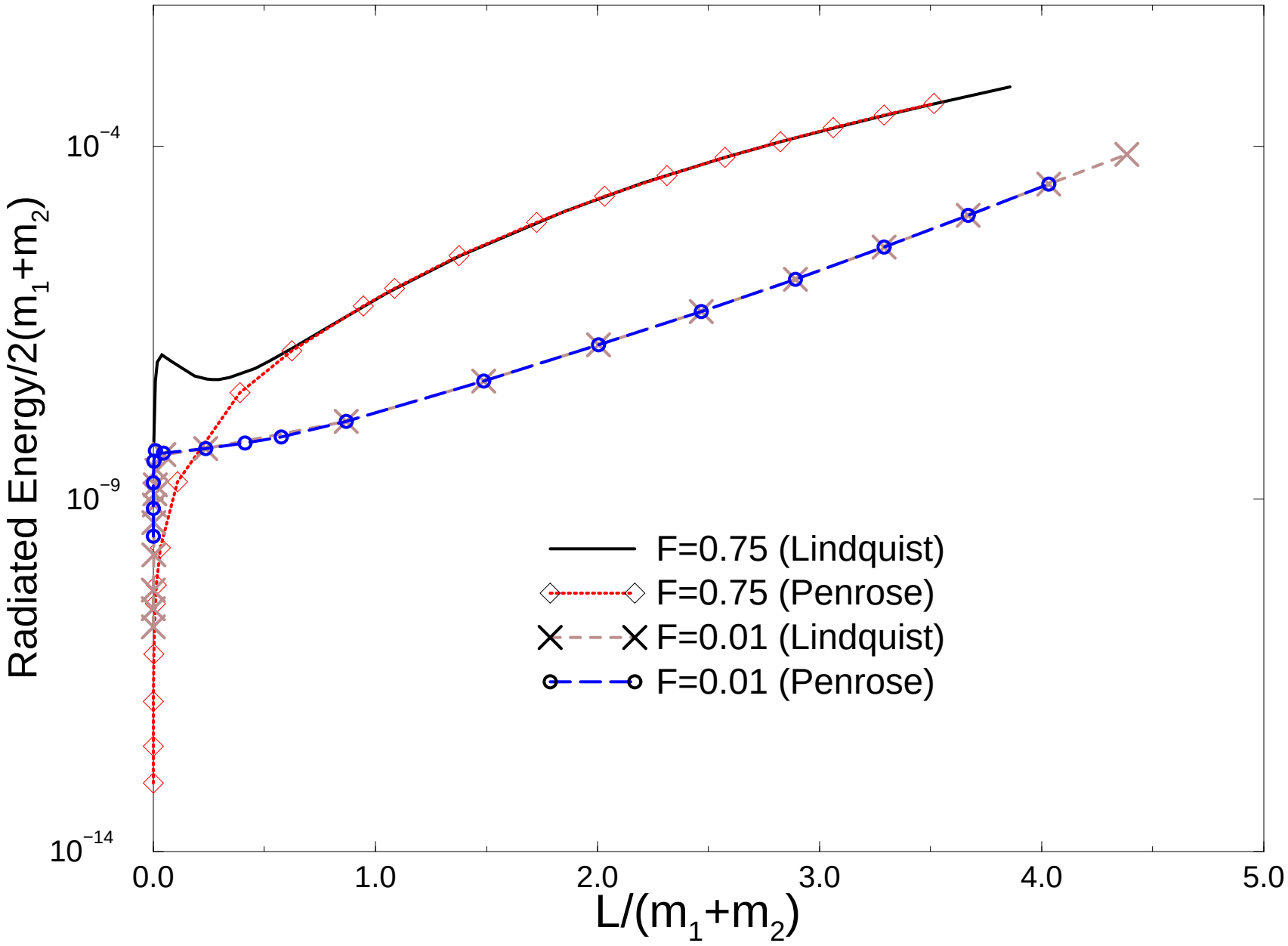
Radiated Energy/2(m1+m2)
10−4
10−9
10−14
0.0
1.0
2.0
3.0
4.0
5.0
L/(m1+m2)
F=0.75 (Lindquist)
F=0.75 (Penrose)
F=0.01 (Lindquist)
F=0.01 (Penrose)

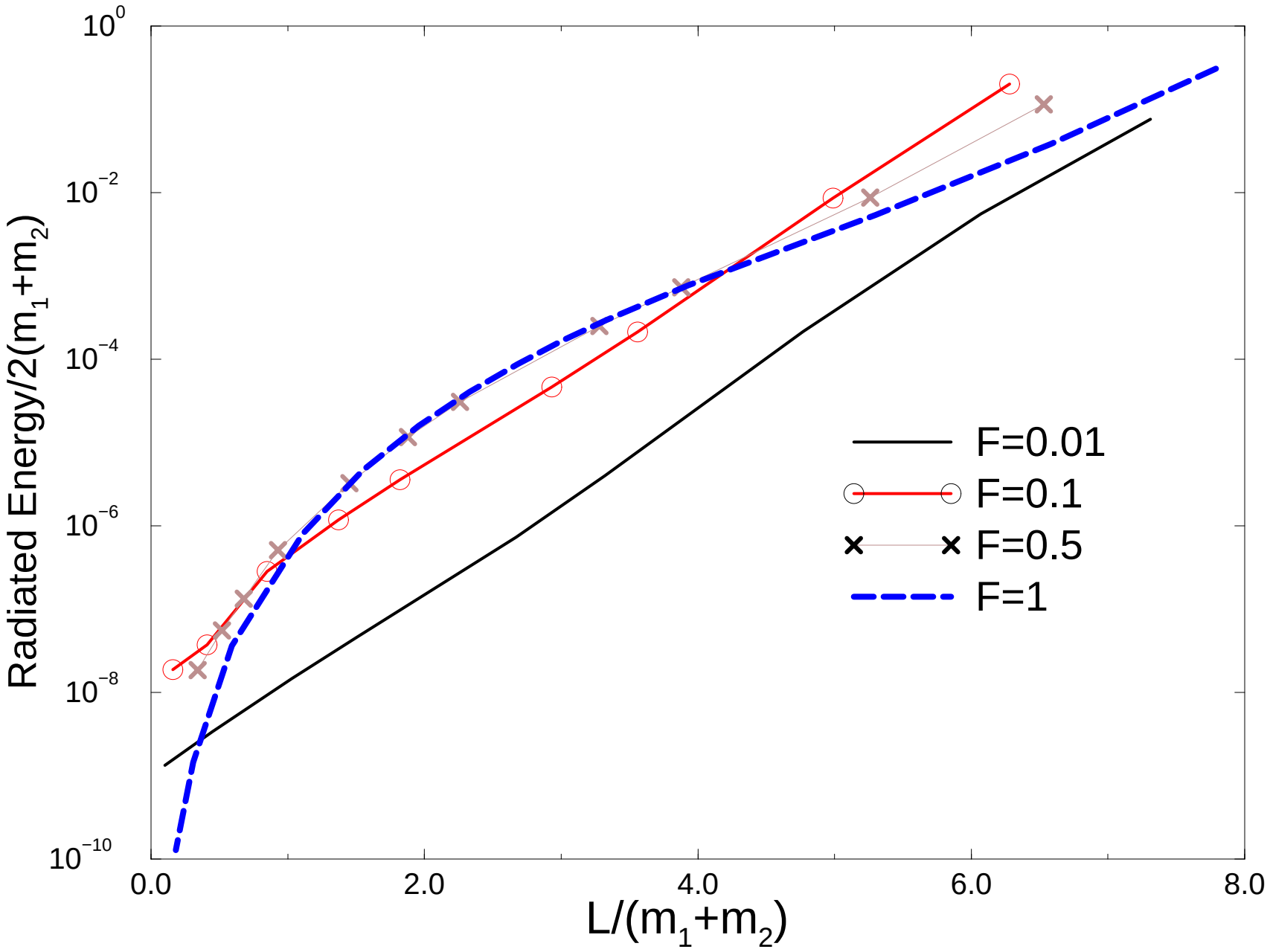
10^{0}
10^{-2}
10^{-4}
10^{-6}
10^{-8}
10^{-10}
Radiated Energy/2(m_1+m_2)
0.0
2.0
4.0
6.0
8.0
L/(m_1+m_2)
F=0.01
F=0.1
F=0.5
F=1

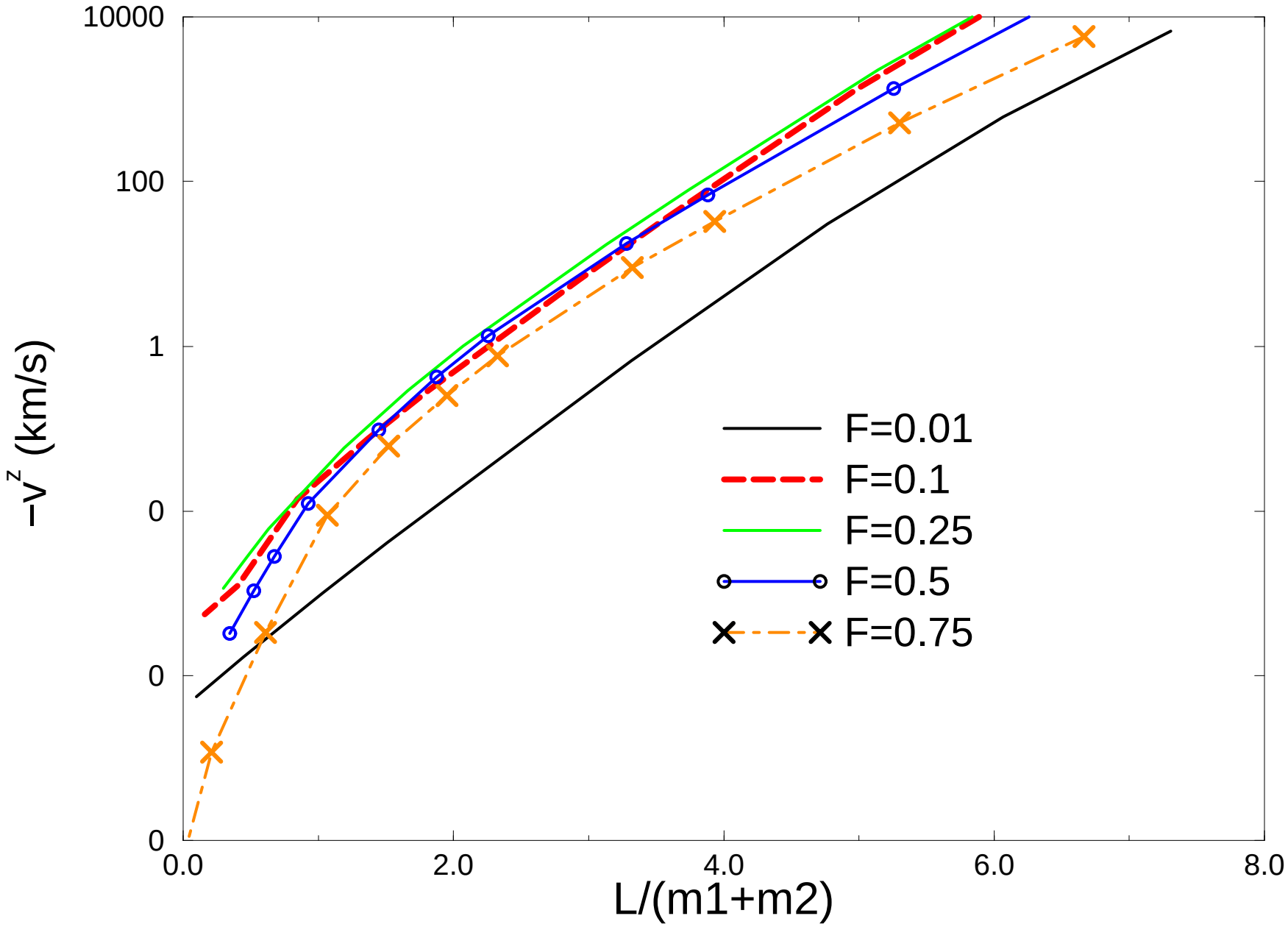
10000
100
1
0
0
0.0
2.0
4.0
6.0
8.0
$-v^z$ (km/s)
L/(m1+m2)
F=0.01
F=0.1
F=0.25
F=0.5
F=0.75

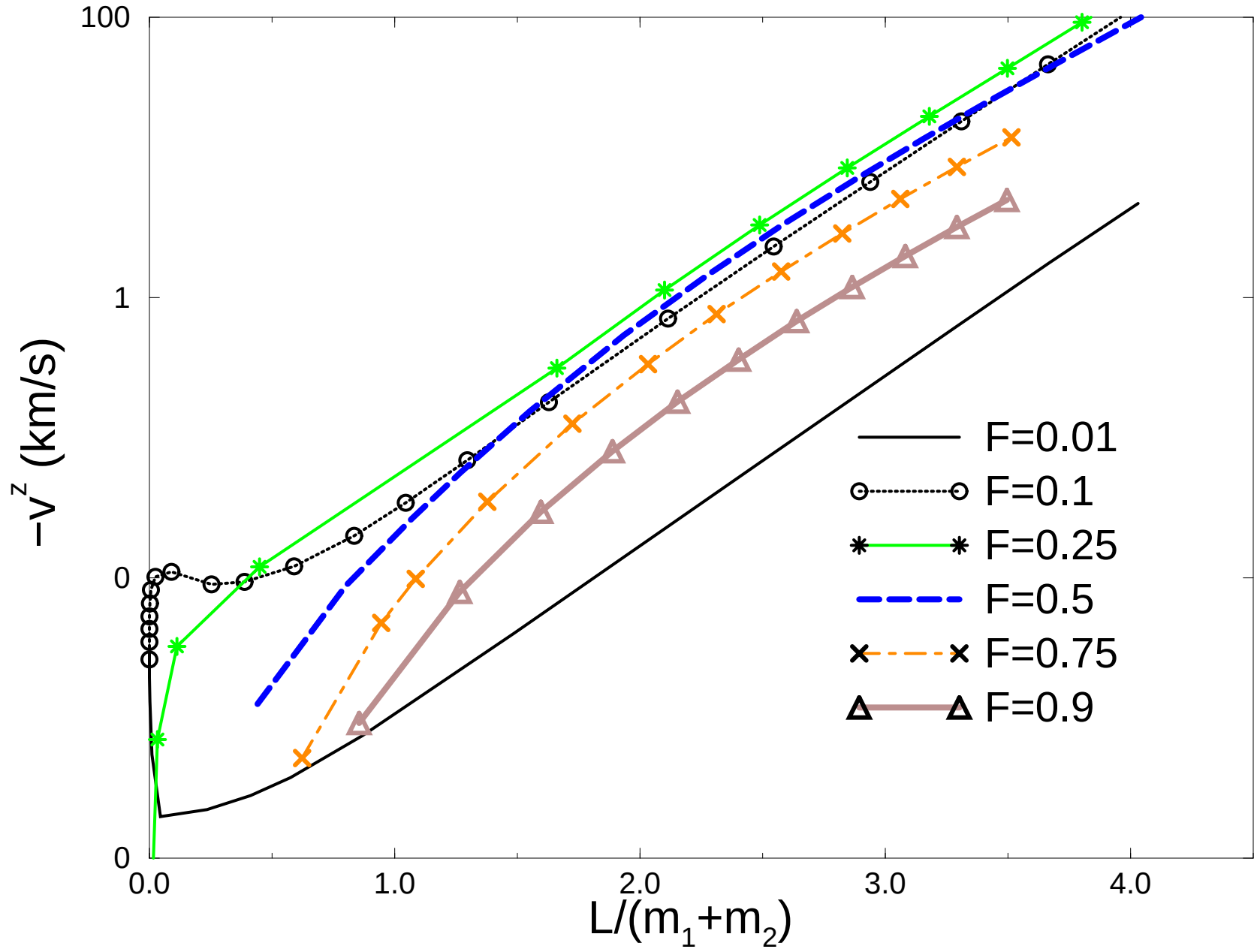
100
1
0
0
$-v^z$ (km/s)
0.0
1.0
2.0
3.0
4.0
$L/(m_1+m_2)$
F=0.01
F=0.1
F=0.25
F=0.5
F=0.75
F=0.9

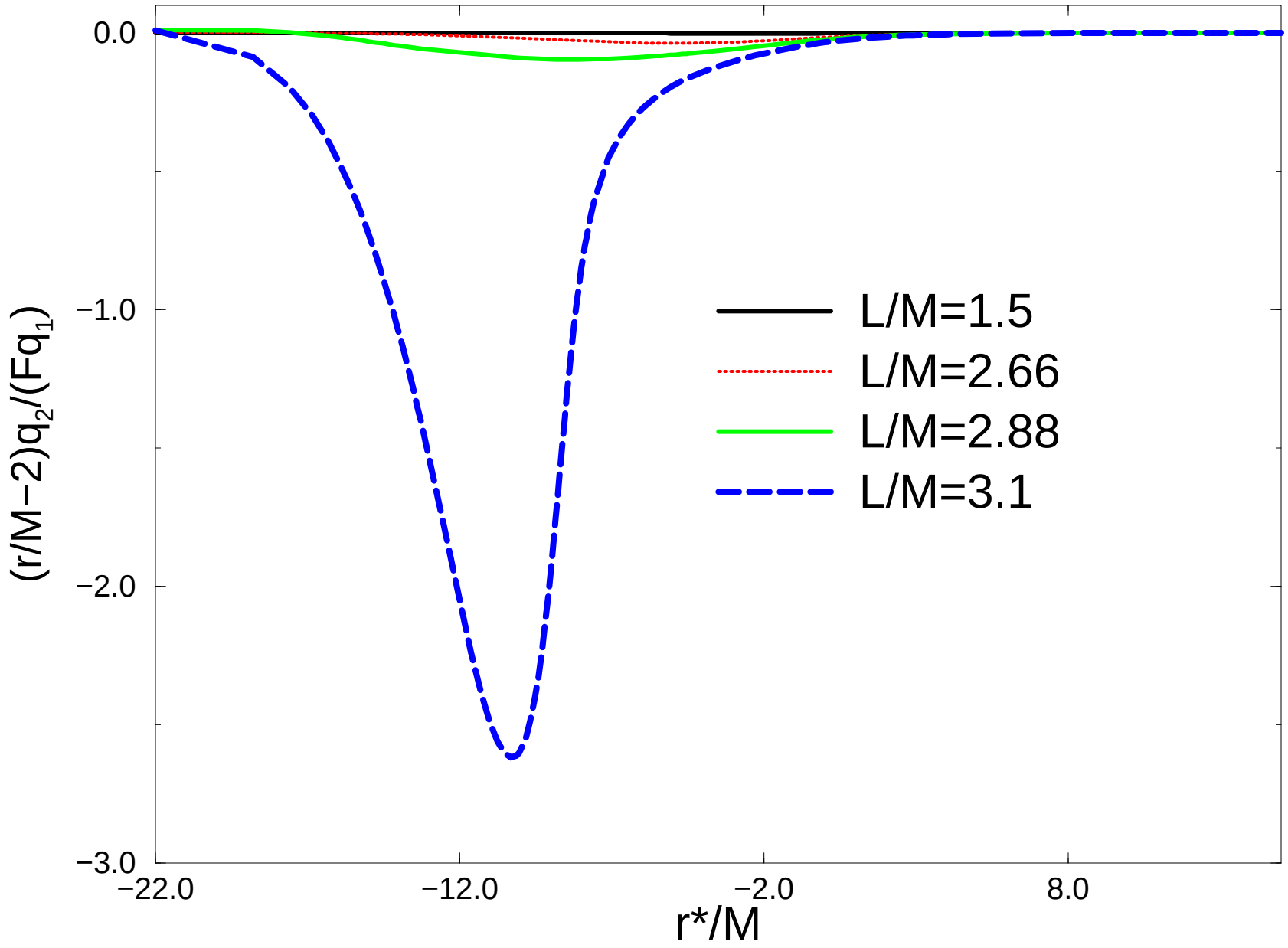
0.0
−1.0
−2.0
−3.0
−22.0
−12.0
−2.0
8.0
r*/M
(r/M−2)q2/(Fq1)
L/M=1.5
L/M=2.66
L/M=2.88
L/M=3.1

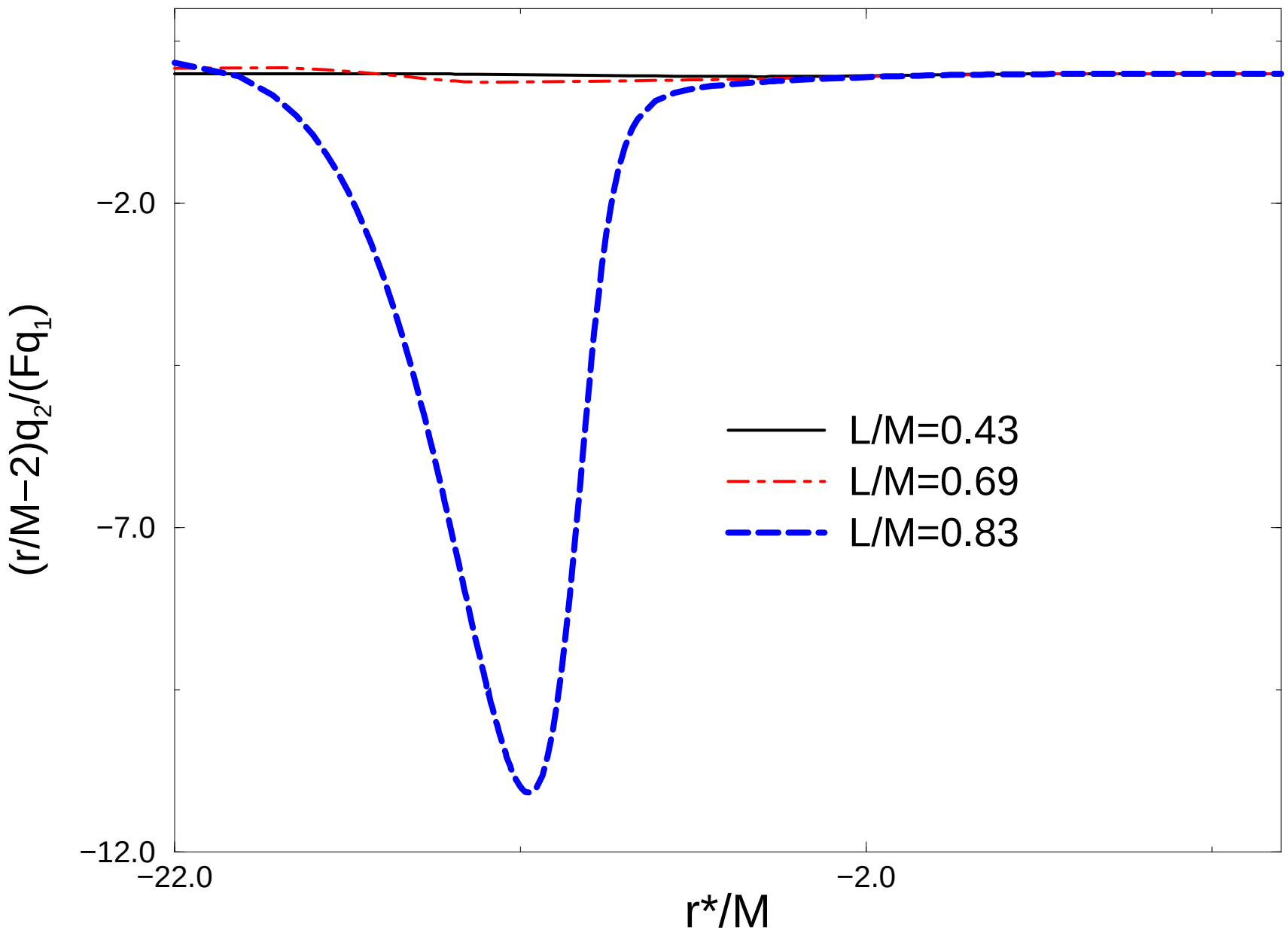
−2.0
−7.0
−12.0
−22.0
−2.0
r*/M
(r/M−2)q2/(Fq1)
L/M=0.43
L/M=0.69
L/M=0.83